FEBS Letters 589 (2015) 131–137

FEBS Letters

journal homepage: www.FEBSLetters.org

# Crystal structure of the catalase–peroxidase KatG W78F mutant from *Synechococcus elongatus* PCC7942 in complex with the antitubercular pro-drug isoniazid

Saori Kamachi [a], Kei Hirabayashi [b,c], Masahiro Tamoi [d], Shigeru Shigeoka [d], Toshiji Tada [a,*], Kei Wada [b,*]

[a] Graduate School of Science, Osaka Prefecture University, Sakai, Osaka 599-8531, Japan
[b] Organization for Promotion of Tenure Track, University of Miyazaki, Miyazaki 889-1692, Japan
[c] Graduate School of Science, Osaka University, Toyonaka, Osaka 560-0043, Japan
[d] Faculty of Agriculture, Kinki University, Nakamachi, Nara 631-8505, Japan

ARTICLE INFO

*Article history:*
Received 9 October 2014
Revised 21 November 2014
Accepted 23 November 2014
Available online 3 December 2014

Edited by Stuart Ferguson

*Keywords:*
Crystal structure
Catalase–peroxidase
KatG
Isoniazid

ABSTRACT

**Isoniazid (INH) is a pro-drug that has been extensively used to treat tuberculosis. INH is activated by the heme enzyme catalase–peroxidase (KatG), but the mechanism of the activation is poorly understood, in part because the INH binding site has not been clearly established. Here, we observed that a single-residue mutation of KatG from *Synechococcus elongatus* PCC7942 (*Se*KatG), W78F, enhances INH activation. The crystal structure of INH-bound KatG-W78F revealed that INH binds to the heme pocket. The results of a thermal-shift assay implied that the flexibility of the *Se*KatG molecule is increased by the W78F mutation, allowing the INH molecule to easily invade the heme pocket through the access channel on the γ-edge side of the heme.**


## 1. Introduction

Isoniazid (INH) is a pro-drug that has been extensively used as a first-choice drug for the tuberculosis chemotherapy. A decade-long genetic and biochemical investigations revealed that INH is activated by the catalase–peroxidase KatG of *Mycobacterium tuberculosis* [1–3]. Originally, KatG proteins were identified as bi-functional heme enzymes belonging to the class I peroxidase family. In contrast to monofunctional peroxidases, these enzymes exhibit both catalase activity and broad-spectrum peroxidase activity. The INH activation ability of KatG was identified by analysis of an INH-resistant *M. tuberculosis* species [1]. During activation, the INH molecule is cleaved by KatG to generate an isonicotinyl radical (IN·); subsequently, in the presence of superoxide, the IN· radical combines with $NAD^+$ to generate an isonicotinyl-NAD (IN·NAD) covalent adduct [4]. The IN·NAD adduct inhibits the InhA enzyme, which is involved in the synthesis of mycolic acid [2], a major unique component of the mycobacterial cell wall. In contrast to the inhibitory mechanism of InhA by IN·NAD adduct [2], which has been clearly elucidated, the detailed mechanisms of INH activation by KatG remain unclear, and the exact binding site of INH on KatG is unknown.

The mechanisms of INH activation have been explored not only in *M. tuberculosis* KatG (*Mt*KatG) [5–7] but also in other KatGs such as those of *Burkholderia pseudomallei* (*Bp*KatG) [4,8–10], *Synechocystis* PCC 6803 (*Syn*KatG) [11–13] and *Synechococcus elongatus* PCC7942 (*Se*KatG) [14]. These KatGs share at least 54% sequence identity, and their overall structures are very similar [15–17]. In addition, the configuration of the residues around the heme, including the unique covalent bonds among the side chains of the Met–Tyr–Trp residues of KatG, located on the distal side of the heme, are found in KatG proteins from all three species. Therefore, the environments of the heme pocket in *Mt*KatG, *Bp*KatG, *Syn*KatG and *Se*KatG are believed to be almost identical.

To date, information regarding the INH binding site of KatG has primarily been obtained by spectroscopic studies. The results of

*Abbreviations:* APX, ascorbate peroxidase; ARP, *Arthromyces ramosus* peroxidase; *Bp*KatG, *Burkholderia pseudomallei* KatG; CCP, cytochrome *c* peroxidase; HRP, horseradish peroxidase; INH, isoniazid; *Mt*KatG, *Mycobacterium tuberculosis* KatG; *Se*KatG, *Synechococcus elongatus* PCC7942 KatG; *Syn*KatG, *Synechococcus* PCC6803 KatG

* Corresponding authors. Fax: +81 72 254 9935 (T. Tada), +81 985 85 0873 (K. Wada).
*E-mail addresses:* tada@b.s.osakafu-u.ac.jp (T. Tada), keiwada@med.miyazaki-u.ac.jp (K. Wada).

http://dx.doi.org/10.1016/j.febslet.2014.11.037

the experiments performed so far suggest that the INH binding/activation process occurs in the vicinity of the heme: Raman spectroscopy intensities reveal that upon treatment with INH, the binding of INH perturbs bound CO in the distal heme pocket of *Mt*KatG [18]; similarly, the characteristic UV–visible spectrum of the oxoferryl species (Fe(IV)=O) in *Bp*KatG changes rapidly upon addition of INH [4]. In addition, electron paramagnetic resonance spectroscopy demonstrated that the heme-derived signal changes upon addition of INH [19].

Interestingly, electron paramagnetic resonance (EPR) experiments clearly demonstrated that KatG has several sites of the radical intermediate in the enzymatic reaction, and the site was differ among the KatGs; in the *Mt*KatG [Fe(IV)=O Trp$^{\cdot}$] species was the reactive intermediate with the INH reaction [20], whereas in the *Syn*KatG the first committed intermediate, identified as the Trp$^{\cdot}$ and a Tyr$^{\cdot}$, formed subsequently to the stable [Fe(IV=O) Porphyrin$^{\cdot+}$] species by intermolecular electron transfer [13]. More recently, we determined the structure of the INH-bound *Se*KatG [14], which revealed that three INH molecules are weakly bound to the molecular surface (Fig. 1); one INH molecule was bound at the entrance to the ε-edge side of heme (Site 1). Another was bound at the entrance to the γ-edge side of heme (Site 2), and the other was bound to the loop structures in front of the heme propionate side chain (Site 3). All of the interactions between KatG and the bound INH seemed to be weak, mediated mainly by van der Waals contacts. In contrast, crystallographic analysis of INH-bound *Bp*KatG demonstrated that one INH molecule binds to the molecular surface at the dimer interface, a site that is ~20 Å distant from the entrance to the heme cavity [4]. Subsequent mutation experiments demonstrated that the residues involved in INH binding, as revealed by the structure, had no effect on INH activation; therefore, this remote site is not the only binding site for INH [4]. Taken together, the INH-binding sites of *Se*KatG and *Bp*KatG are probably different, and the exact binding site of INH on KatG is still controversial.

During the course of a mutational study of *Se*KatG, aimed at investigating the localization of the radical during the reaction, we observed that a single-residue mutation in *Se*KatG, W78F, enhanced INH activation. The mutated tryptophan residue (W78), which is highly conserved in all KatG orthologues, is located at the entrance of the γ-edge side of the heme (Site 2) [15–17,21]. The side chain of the tryptophan shielded the γ-edge–side heme-access channel, and thus seemed to function as the "lid" of the heme pocket. In order to gain a better understanding of INH recognition/binding, we determined the crystal structures of the *Se*KatG-W78F mutant protein. The single-residue mutation resulted in dramatic alteration of the INH-binding site relative to that of the wild type: in *Se*KatG-W78F, the INH molecule bound in the heme pocket, whereas in wild-type *Se*KatG, three INH molecules bound on the molecular surface.

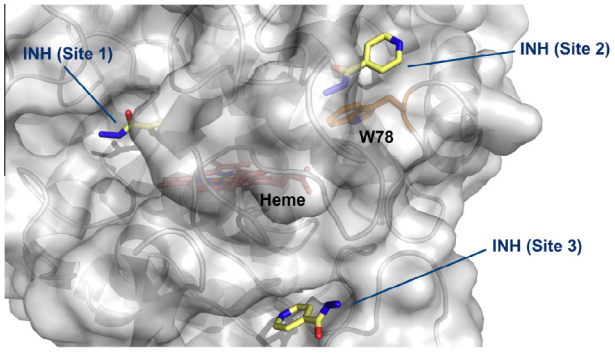


**Fig. 1.** The locations of the INH-binding sites in the wild-type *Se*KatG. The wild-type *Se*KatG has three low-affinity INH binding sites (Site 1–3). Three INH molecules bound on the molecular surface via van der Waals contacts. The molecular surface drawing is overlain with the cartoon drawing of the INH-bound wild-type *Se*KatG (PDB ID: 3WXO). The bound INH molecules and heme are shown in yellow and pink. Trp78 is shown in orange.

## 2. Materials and methods

### 2.1. Expression, purification, and characterization

Oligonucleotide-directed mutagenesis of Trp78 to Phenylalanine in *Se*KatG was performed by overlap extension PCR using the pET-3a plasmid containing the *Se*KatG gene as the template [17]. The oligonucleotide pair 5′-CCAAGACTGGTTTCCGGCAG-ACTG-3′ and 5′-CAGTCTGCCGGAAACCAGTCTTGG-3′ was used to produce the *Se*KatG-W78F mutant. The plasmids were transformed into *Escherichia coli* strain BL21(DE3). Protein overexpression and purification were carried out as described for native *Se*KatG [22].

### 2.2. Crystallization, X-ray diffraction data collection, and structure determination

Crystals of *Se*KatG-W78F were successfully obtained under the same conditions (4.3 M sodium formate, with 0.1 M sodium citrate [pH 6.3] as a precipitant) used for the native *Se*KatG. INH-bound crystals were prepared by soaking the crystals of *Se*KaG-W78F in crystallization solution containing 100 mM INH for 12 h. On beamline BL44XU at SPring-8 (Japan Synchrotron Radiation Research Institute), X-ray diffraction data of INH-bound and INH-free *Se*KatG-W78F were obtained to 3.2 Å and 2.65 Å resolution, respectively, from a flash-cooled crystal, which did not require

**Table 1**
Data collection and crystallographic analysis.*

| | INH-bound KatG-W78F | INH-free KatG-W78F |
|---|---|---|
| *Data collection* | | |
| Beamline | SPring-8 BL44XU | SPring-8 BL44XU |
| Space group | $P4_12_12$ | $P4_12_12$ |
| *Unit cell* | | |
| *a*, *b*, *c* (Å) | 107.7, 107.7, 204.8 | 108.3, 108.3, 203.3 |
| α, β, γ (°) | 90.0, 90.0, 90.0 | 90.0, 90.0, 90.0 |
| Wavelength (Å) | 0.9000 | 0.9000 |
| Resolution (Å) | 50.0–3.20 (3.31–3.20) | 50.0–2.65 (2.74–2.65) |
| Completeness (%) | 99.8 (99.8) | 99.9 (99.4) |
| Redundancy | 5.2 (4.6) | 6.8 (6.4) |
| $I/\sigma$ (I) | 16.3 (3.0) | 10.4 (5.7) |
| $R_{merge}$† | 0.111 (0.532) | 0.169 (0.491) |
| *Refinement* | | |
| Resolution (Å) | 50.0–3.20 | 50.0–2.65 |
| No. of reflections | 19354 | 33798 |
| $R/R_{free}$‡ | 0.180/0.260 | 0.196/0.254 |
| RMSD bond lengths (Å) | 0.01 | 0.017 |
| RMSD bond angles (°) | 1.52 | 1.92 |
| Average *B* value (Å$^2$) | 73.1 | 49.3 |
| *Ramachandran plot* | | |
| Most favored region (%) | 90.8 | 87.9 |
| Additionally allowed regions (%) | 7.8 | 12.1 |
| Generously allowed regions (%) | 1.4 | 0 |
| PDB ID | 4PAE | 3X16 |

* The statistics in the highest-resolution shell are given in parentheses.
† $R_{merge} = \Sigma_{hkl}\ \Sigma_i\ |I_i(hkl) - \langle I(hkl)\rangle|/\Sigma_{hkl}\Sigma_i\ I_i(hkl)$, where $I_i(hkl)$ is the observed intensity and $\langle I(hkl)\rangle$ is the average intensity for multiple measurements.
‡ $R = \Sigma_{hkl}\ ||F_{obs}| - |F_{calc}||/\Sigma_{hkl}\ |F_{obs}|$, where $F_{obs}$ is the observed structure factor and $F_{calc}$ is the calculated structure factor. $R_{free}$ is the same as *R*, except calculated using 5% of the data that were not included in any refinement calculations.

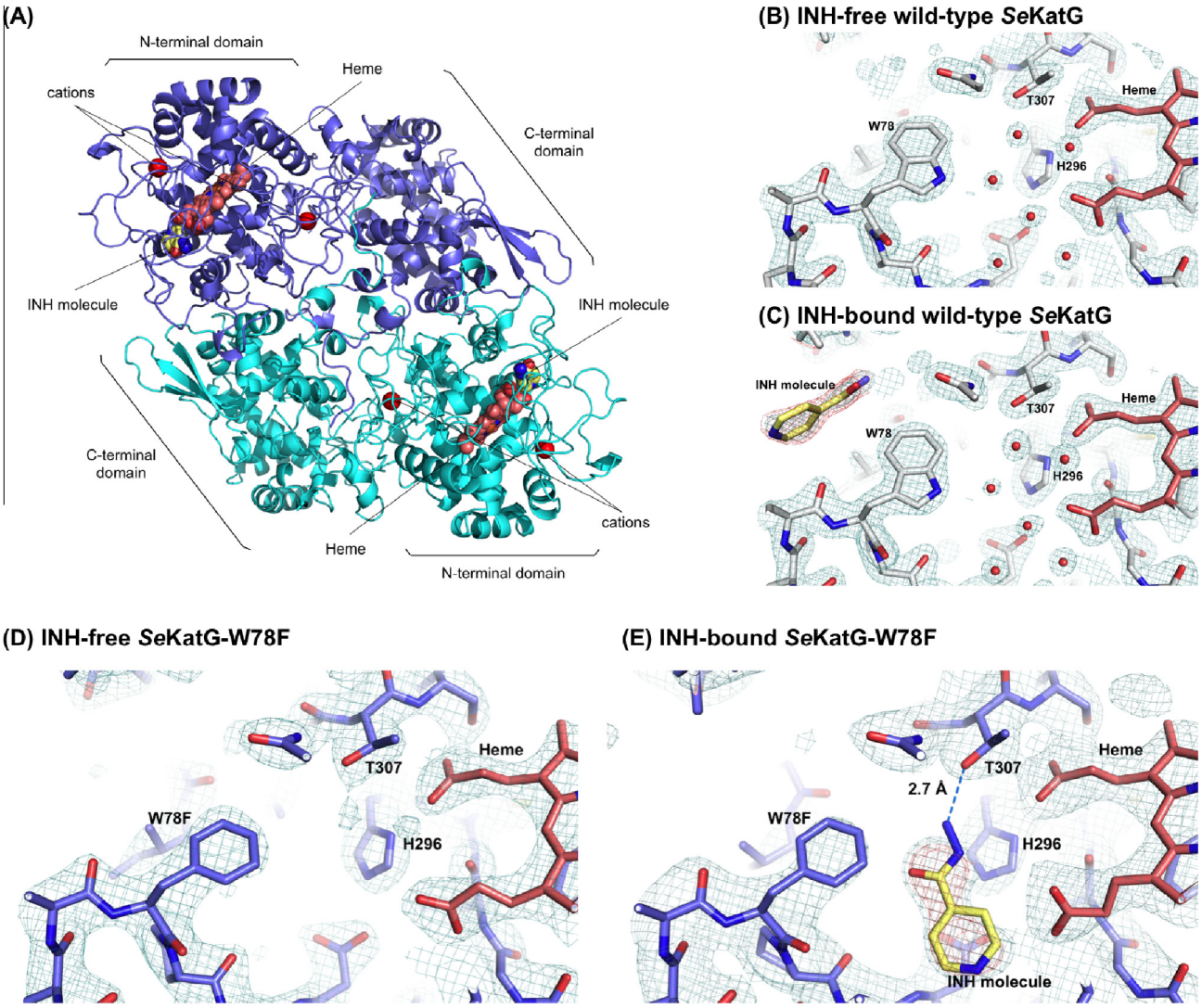


**Fig. 2.** Crystal structure of *Se*KatG-W78F in complex with INH, and a comparison of the heme cavity between the wild type and W78F mutant. (A) Overall structure of INH-bound *Se*KatG-W78F. The dimeric structure of *Se*KatG-W78F was generated via a symmetry operation using the crystallographic 2-fold axis. The individual subunits are shown in purple or cyan. The bound INH molecules, hemes, and cations are shown in yellow, pink, and red, respectively. (B–E) Comparison of the electron-density maps of the INH-free wild-type *Se*KatG (PDB ID: 3WNU), INH-bound wild-type *Se*KatG (PDB ID: 3WXO), INH-free *Se*KatG-W78F (PDB ID: 3X16) and INH-bound *Se*KatG-W78F. An $F_o$–$F_c$ map omitting the INH molecule, contoured at 3.0$\sigma$ (red), is overlaid on a stick model of the bound INH. Water molecules are shown as red balls, and the blue broken line indicates a hydrogen bond.

the addition of other cryoprotectants. The data set was processed and scaled using the *HKL-2000* package [23].

Crystals of INH-bound *Se*KatG-W78F were nearly isomorphous with those of native KatG, and the structure of *Se*KatG-W78F was determined using the structure of the native KatG (PDB ID: 3WNU) as a model [17]. The structure was subjected to rigid-body refinement using Refmac5 [24] from the CCP4 package [25]. The structure was further refined by restrained refinement in Refmac5, and manual model revision was carried out using COOT [26]. The electron-density map at the final stage was clear enough to precisely assign the orientation of the bound INH molecules. Details of the data collection and refinement statistics are summarized in Table 1. The coordinates and structure factors have been deposited at the RCSB Protein Data Bank under accession codes 4PAE (INH-bound *Se*KatG) and 3X16 (INH-free *Se*KatG).

### 2.3. Enzymatic IN·NAD formation by SeKatG W78F

IN·NAD formation activity was assayed at 37 °C using a reaction mixture containing 0.4 mM $NAD^+$, 1.0 mM INH, 2 μM $MnCl_2$, 50 mM Tris–HCl (pH 7.8), and 50 μg/ml enzyme. IN·NAD formation was monitored at 326 nm ($\varepsilon = 6900\ M^{-1}\ cm^{-1}$) using a V630BIO spectrometer (JASCO). $K_m$ values for INH were determined using reaction mixtures containing various concentrations of INH (0.5, 1.25, 2.5, 5, 10, 20, 40 mM). The non-enzymatic reaction was estimated using the same reaction mixture without enzyme, and the result was used for the background value in calculations of enzymatic activity. The enzyme kinetic parameters were estimated by non-linear least-squares curve fitting in Microsoft Excel Solver.

### 2.4. Thermal shift assays of SeKatG-W78F

Thermal shift assays were performed on a CFX96 Real-Time PCR Cycler (Bio-Rad Laboratories). In a typical experiment, 1 μl of SYPRO Orange (Sigma–Aldrich, diluted from 5000× stock into 50 mM Tris–HCl, pH 7.8), 4 μl protein (0.4 mg/ml), and 5 μl buffer (50 mM Tris–HCl, pH 7.8) were mixed on ice in a white 96-well PCR plate (Bio-Rad Laboratories). To evaluate the effect of INH binding, 1 μl of 5000× SYPRO Orange, 4 μl protein (0.4 mg/ml), 1 μl INH (10 mM), and 4 μl Tris–HCl buffer were mixed. Fluorescence was

**Table 2**
Steady-state kinetics of IN·NAD formation by wild-type *Se*KatG and *Se*KatG-W78F.

| | Apparent specific activity[a] (nmol/min/mg protein) | $k_{cat}$[b] ($min^{-1}$) | $K_m$ INH (mM) | $k_{cat}/K_m$ ($S^{-1}$ $mM^{-1}$) |
|---|---|---|---|---|
| *Se*KatG wild-type | 33.3 ± 6.3 | 43.9 | 5.6 | 0.13 |
| *Se*KatG W78F | 131.8 ± 8.7 | 38.8 | 1.3 | 0.50 |

[a] The apparent specific activities were evaluated at 37 °C using a reaction mixture containing 0.4 mM $NAD^+$, 1.0 mM INH, 2 μM $MnCl_2$, 50 mM Tris–HCl, pH 7.8. The *Se*KatG and it variant concentrations were determined by using the absorbance at 280 nm ($\varepsilon$ = 177 270 $M^{-1}$ $cm^{-1}$).
[b] The turnover number is defined as that rate at which the enzyme can produce IN·INH per heme per unit time. The bound heme concentration was determined by using the absorbance at 405 nm ($\varepsilon$ = 100 $mM^{-1}$ $cm^{-1}$).

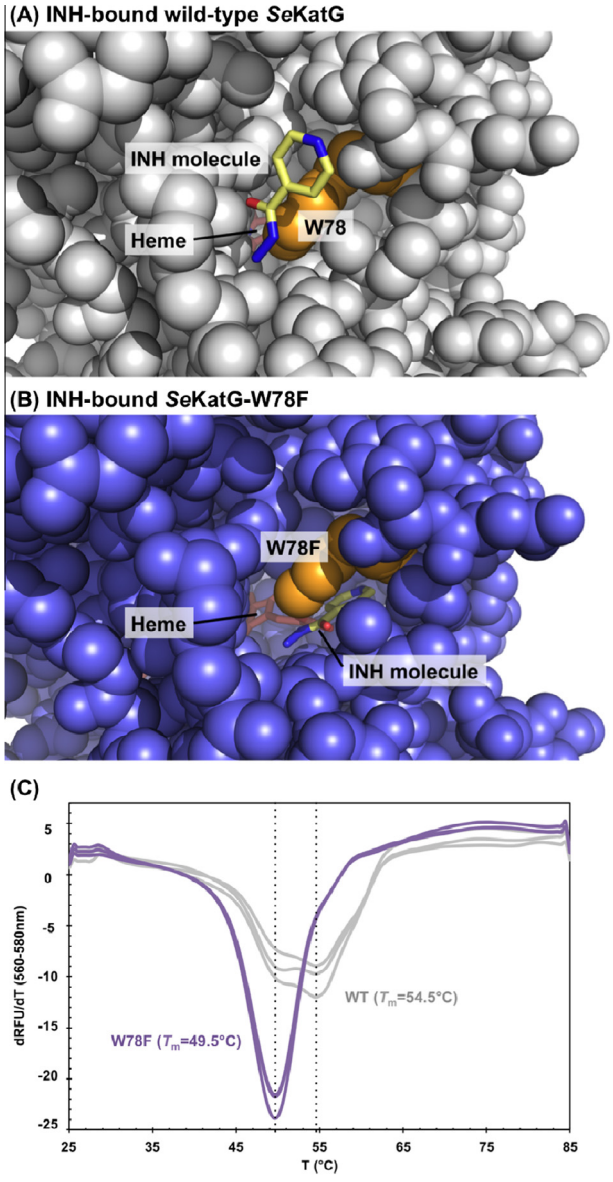


**Fig. 3.** Alteration of *Se*KatG by introduction of the W78F mutation. (A and B) A structural comparison of the entrance of the γ-edge side of heme in the INH-bound forms of wild-type *Se*KatG and *Se*KatG-W78F. Residue 78 (the mutated site) is shown in orange. The bound INH molecule and heme are shown in yellow and pink. (C) Thermal-shift assays of the wild type and W78F mutant. Inverse first-derivative plots of wild type (white) and W78F (purple). Average $T_m$ values are shown alongside each curve. $n$ = 3 for each assay.

measured from 25 °C to 85 °C in 0.5 °C steps (excitation, 450–490 nm; detection, 560–580 nm). All measurements were performed three times. Data evaluation and melting-point determination were conducted using the Bio-Rad CFX Manager software.

## 3. Results and discussion

### 3.1. Overall structure of SeKatG-W78F

The structure of INH-bound *Se*KatG-W78F was refined at 3.2 Å resolution to $R$ and $R_{free}$ values of 0.18 and 0.26, respectively. The asymmetric unit contained one subunit of a *Se*KatG molecule including a protoporphyrin IX heme moiety, and two cations (modeled as sodium ions). The crystallographic equivalent subunit was created by a 2-fold symmetry operation to form the functional dimer (Fig. 2A). Although the electron density for *Se*KatG-W78F was mostly continuous, the densities for the N-terminal segment (residues 1–11) and C-terminal segment (719–720) were poorly defined; accordingly, these residues were not included in the model. When the structure of INH-bound *Se*KatG-W78F was superposed on that of the INH-free *Se*KatG, no significant structural changes were observed in the enzyme; the root-mean-square (rms) deviation for the $C_\alpha$ atoms was 0.37 Å.

### 3.2. Binding site of the INH molecule in SeKatG-W78F

The electron-density map of *Se*KatG-W78F was slightly obscured due to the low-resolution data (3.2 Å), but comparison of the electron-density maps unambiguously revealed the binding position of the INH molecule. In the case of the INH-free wild-type *Se*KatG (Fig. 2B) [17] and INH-bound wild-type *Se*KatG (Fig. 2C) [14], the map around the heme propionate moiety clearly showed that water molecules occupied in this space. By contrast, the $F_o$–$F_c$ map of the *Se*KatG-W78F crystal soaked with INH solution revealed a positive density (>3$\sigma$) at the corresponding position (Fig. 2E). In the same manner, we confirmed that the $F_o$–$F_c$ maps of *Se*KatG-W78F crystals soaked with or without the INH solution yielded consistent results (Fig. 2D and E). Thus, we attributed the electron density in the $F_o$–$F_c$ map to the bound INH molecule. The bound INH molecule was held in position in the space between the propionate moiety of heme and Phe78 by a hydrogen bond: the distance between the O atom of the Thr307 hydroxyl moiety and the N3 atom of the INH hydrazide moiety was 2.7 Å. Namely, the INH molecule was trapped inside the heme pocket in *Se*KatG-W78F.

In the structure of INH-bound wild-type *Se*KatG determined at 2.12 Å resolution [14], we could assign three INH molecules, but all of the bound INH molecules were located on the protein surface (Fig. 1). In addition, all interactions between KatG and the bound INH molecules seemed to be weak, mediated only by van der Waals contacts. Therefore, the one-residue substitution of W78F in *Se*KatG dramatically changed the INH binding site.

### 3.3. Enzymatic and structural alterations of SeKatG by introducing the W78F mutation

The steady-state kinetics of INH activation revealed that the $k_{cat}$ values were almost unchanged by introducing the W78F mutation (Table 2), though this mutation slightly increased the affinity (decrease in $K_m$ value) of KatG for INH by more than 4-fold relative to the wild type. Thus, it is likely that the Trp78 residue is not directly involved in the catalytic reaction of the INH activation,

but instead hampers invasion of the heme pocket by the INH molecule. This result is probably consistent with the reported EPR results that [Fe(IV)═O Trp106· (corresponding to the W78 in *Se*KatG)] did not involved in the reaction with INH [13].

In the structure of INH-bound wild-type *Se*KatG, one INH molecule was bound to the outside of the entrance of heme pocket and interacted with W78 residue via a van der Waals contact (Fig. 3A) [14]; apparently, this INH molecule was unable to enter the heme pocket due to steric obstruction by the lid residue Trp78, which is located at the entrance on the γ-edge side of the heme. In the W78F mutant, the bulky side-chain of the indole ring of Trp is replaced by the slightly smaller benzyl ring of Phe. We assumed that changing the lid residue in this manner would enlarge the access channel. As expected, structural comparison between the wild type and W78F demonstrated that in *Se*KatG-W78F the access channel was slightly enlarged, and the heme could be seen appreciably from the outside (Fig. 3B); by contrast, in the wild type, the access channel was almost covered by the W78 residue. The entrance size of the access channel in SeKatG-W78F was estimated to about 4.7 Å (width) × 1.2 Å (height), based on van der Waals radii. Thus, the entrance may be too small for the INH molecule to invade the heme pocket; based on the size of the INH molecule, entry would require an entrance of at least 6 Å (width) × 3.5 Å (height).

A thermal-shift assay provided insight into how the INH molecule could enter the heme pocket despite the restricted size of the access channel (Fig. 3C). The denaturing temperature curve for *Se*KatG dramatically changed upon introduction of the W78F mutation; wild-type *Se*KatG exhibited a bi-modal curve, in which the thermal denaturation temperatures ($T_m$) were around 54.5 °C. This bi-modal curve also revealed a local minimum of $T_m$ at 49.5 °C, indicating that the denaturation process (thermal stability states) in wild-type *Se*KatG has two steps or that two different states are present in solution. By contrast, the W78F mutation changed the curve to a mono-modal pattern, with a $T_m$ of 49.5 °C. This change indicates that the W78F mutation affected protein stability. One possible explanation is that the W78F mutation increased the flexibility of the *Se*KatG molecule, so that the INH molecule could easily invade the heme pocket through the access channel on the γ-edge side of heme, even though the channel in the crystalline state was too small.

### 3.4. Structural comparisons among the INH-bound KatG and the canonical peroxidases

To date, several groups have reported that INH molecule(s) can bind in the heme pocket: one study examined the *Bp*KatG-D141A mutant [10], and the other two investigated the plant class I peroxidases [27,28]. The recently reported structure of *Bp*KatG containing the D141A mutation demonstrated that the INH molecule could also enter/bind the heme cavity by removing the lid residue (D141) at the δ-edge entrance to the funnel-shaped heme cavity (Fig. 4A) [10]. In this structure, the N3 nitrogen atom of the INH molecule directly coordinates to the heme iron in the heme pocket. The binding position of INH, as seen in *Bp*KatG-D141A, may be identical to that of hydrogen peroxide, an authentic substrate for peroxidase/catalase reaction, or heme enzyme inhibitors such as cyan or azide. In the cytochrome *c* peroxidase (CCP), a typical class I peroxidase, INH molecule was also bound to the δ-edge of the heme (Fig. 4B), but the position and configuration of the bound

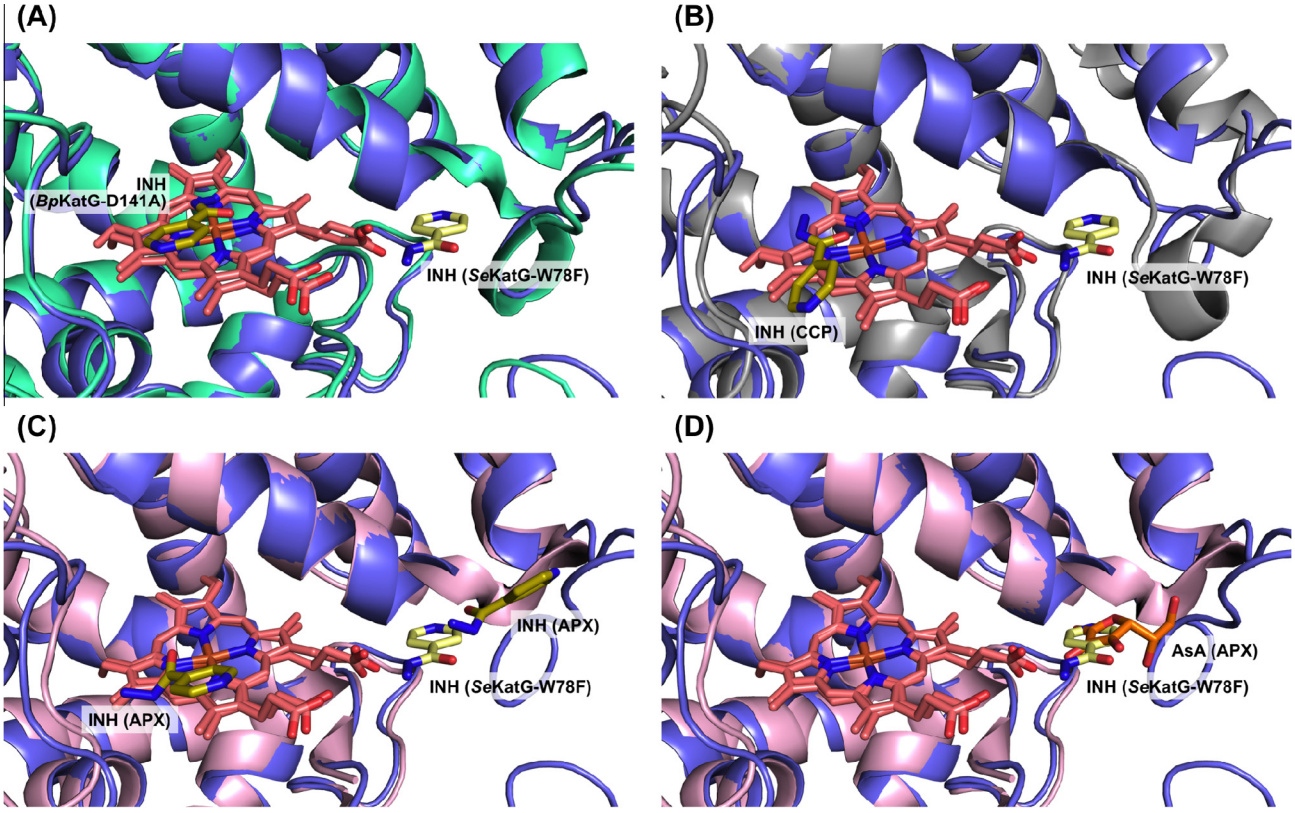


**Fig. 4.** A structural comparison of the INH-binding sites of *Se*KatG-W78F, *Bp*KatG-D141A, CCP and APX. Superposition of the heme pocket in INH-bound *Se*KatG-W78F (purple) and (A) INH-bound *Bp*KatG-D141A (PDB ID: 4KA6 [10]) (green), (B) the INH-bound form of the cytochrome *c* peroxidase CCP (PDB ID: 2V2E [28]) (gray), (C) the INH-bound form of the ascorbate peroxidase APX (PDB ID: 2VCF [28]) (light pink), (D) APX in complex with ascorbate, a physiological electron donor (PDB ID: 1OAF [32]) (light pink). The hemes are shown in pink. The bound INH molecule from *Se*KatG is shown in yellow, and those from *Bp*KatG, CCP and APX are shown in dark yellow. The ascorbate molecule bound in APX is shown in orange.

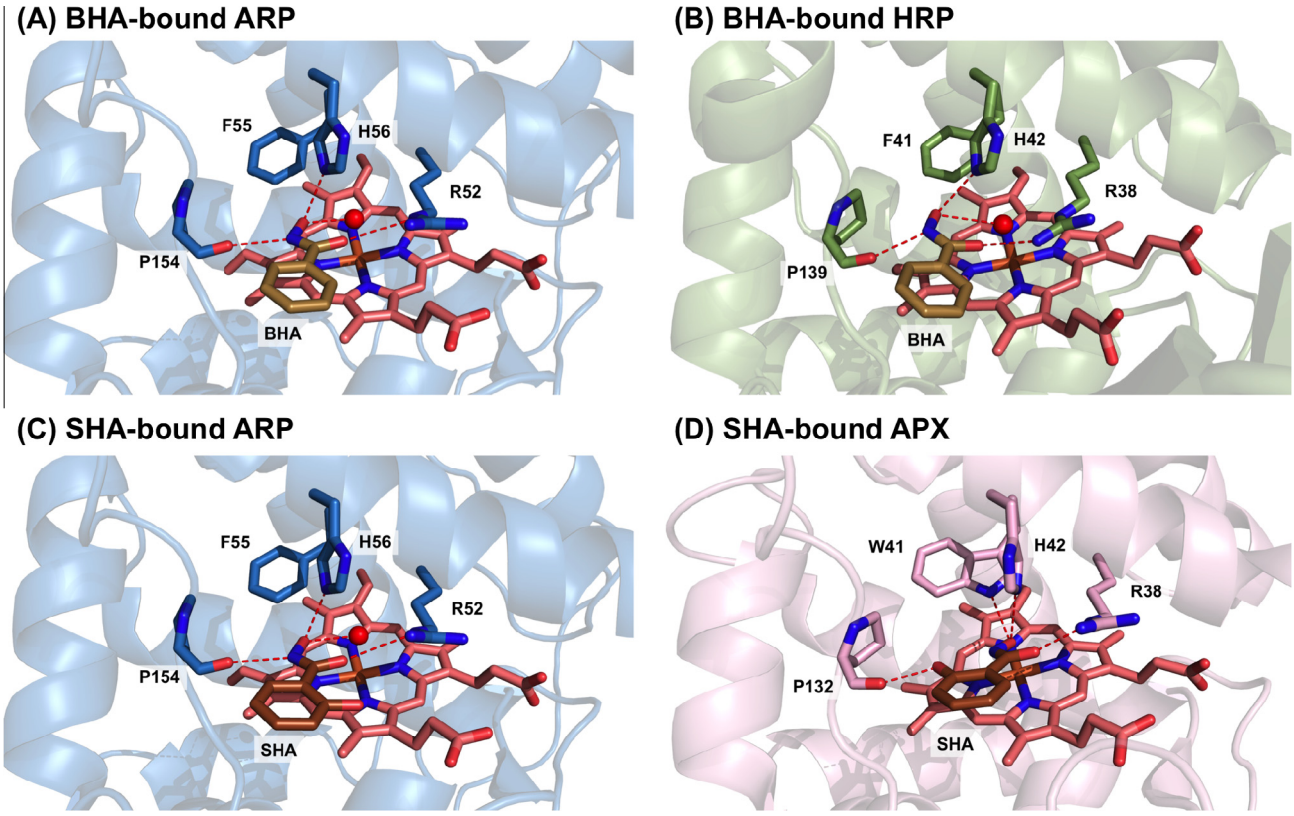


**Fig. 5.** A structural comparison of the BHA/SHA-binding sites of ARP, HRP and APX. The heme cavity in (A) BHA-bound ARP (PDB ID: 1HSR [33]) (blue), (B) BHA-bound HRP (PDB ID: 2ATJ [34]) (moss green), (C) SHA-bound ARP (PDB ID: 1CK6 [35]) (blue), (D) SHA-bound APX (PDB ID: 1V0H [36]) (light pink). The hemes are shown in pink. The bound BHA molecule and SHA molecule are shown in light brown and brown. The ascorbate molecule bound in APX is shown in orange. Water molecules are shown as red balls, and the red broken line indicates a hydrogen bond.

INH was differ from the *Bp*KatG-D141A. On the one hand, in ascorbate peroxidase (APX), a structurally similar class I peroxidase, two INH molecules can also bind in the heme pocket (Fig. 4C) [28]. Although one INH molecule in APX is located at the distal side of the heme, its position/configuration is slightly different from that of the INH in *Bp*KatG-D141A and CCP. The other INH in the APX is near the propionate side chain of the heme. This binding position is similar to that of INH-bound *Se*KatG-W78F.

The peroxidases have a rather low specificity for the electron donor, since they could utilize not only the physiological compound but also the various reagents including the artificial electron donor. The extensive structural studies so far revealed that in the heme pocket of the peroxidases the hydrophobic site(s) exists, and this site functioned as the electron donor binding. For example, the several peroxidases in complex with the benzhydroxamic acid (BHA) or salicylhydroxamic acid (SHA), which is deemed as the structural analogue of INH, have been reported. In most of the peroxidases such as *Arthromyces ramosus* peroxidase (ARP), horseradish peroxidase (HRP) and APX, the aromatic reagents were bound to the δ-edge of the heme pocket [29] (Fig. 5); the configurations of the bound aromatic reagents were similar to each other, indicating the similar environment of the binding site. In the above-mentioned CCP in complex with INH, the INH molecule was also bound to the δ-edge of the heme pocket (Fig. 4B). Notably, in the APX one of the INH molecule as well as the ascorbate, a physiological electron donor, was bound to the γ-edge of the heme pocket (Fig. 4D), as seen in the bound INH in the *Se*KatG W78F.

The access channel of the heme pocket is completely different among the peroxidases and KatGs; the peroxidases have the wide accessible channel to the δ- and γ-edge of the heme, in contrast the wild-type KatG has a closed inaccessible channel even for the small inorganic compound such as the INH. Thus the binding site in *Se*KatG W78F is probably the "pseudo" binding site by introducing the mutation, but this structural result implicates a similar nature between the *Se*KatG and APX, that is, the INH potentially could bind to the γ-edge of the heme. Interestingly, similar to the *Se*KatG, the reported radical intermediate in the APX is [Fe(IV=O) Porphyrin$^{\bullet+}$] specie [30], not a proximal Trp$^{\bullet}$ specie, thus the electron donor binding site may be potentially reflect the radical intermediate site. However, this idea is still highly controversial because several electron-transfer pathways have been reported in KatGs [13,20,31], implying the existence of an alternative INH binding/activating site. In addition, the crystal structure of the INH-bound wild-type *Se*KatG also demonstrated the three INH molecules could bind on the molecular surface [14], all of which are completely different sites in *Mt*KatG. These results strongly implicated that *Se*KatG has the unique INH binding sites as compared to the *Mt*KatG and *Bp*KatG. To reveal the exact reaction mechanism underlying INH activation by each KatG, further spectroscopic, biochemical, and structural studies are needed. The mutational studies will be especially important for the further understanding. Our results here provided the one-residue substitution of W78F in *Se*KatG dramatically changed the INH binding site. Such an unexpected result serves as a cautionary note for mutational experiments in which functional changes of mutated proteins are interpreted without knowledge of their exact structures.

## Acknowledgments

We thank Dr. E. Yamashita and Dr. A. Higashiura for their assistance with data collection at the SPring-8 synchrotron radiation facility (Hyogo, Japan). The synchrotron radiation experiments

were performed on BL38B1 and BL44XU at SPring-8 with the approval of the Japan Synchrotron Radiation Research Institute (Proposal Nos. 2011B6535, 2012B6726, 2013A6828, 2013B6828, 2013B6863, 2014A6963 and 2014B6963). This work was supported by the Program to Disseminate Tenure Tracking (to K.W.) from the Ministry of Education, Culture, Sports, Science, and Technology (MEXT) of Japan; by MEXT Grants-in-Aid of Scientific Research 26440035 (to T.T.) and 5840023 (to K.W.); by a grant from the Japan Foundation for Applied Enzymology (to K.W); and by a Grant-in-Aid for JSPS Fellows 241292 (to K.H.). We thank Y. Motoyama and N. Kaseda of the University of Miyazaki for technical assistance.

## References

[1] Zhang, Y., Heym, B., Allen, B., Young, D. and Cole, S. (1992) The catalase–peroxidase gene and isoniazid resistance of *Mycobacterium tuberculosis*. Nature 358, 591–593.
[2] Rozwarski, D.A., Grant, G.A., Barton, D.H., Jacobs Jr., W.R. and Sacchettini, J.C. (1998) Modification of the NADH of the isoniazid target (InhA) from *Mycobacterium tuberculosis*. Science 279, 98–102.
[3] Rawat, R., Whitty, A. and Tonge, P.J. (2003) The isoniazid-NAD adduct is a slow, tight-binding inhibitor of InhA, the *Mycobacterium tuberculosis* enoyl reductase: adduct affinity and drug resistance. Proc. Natl. Acad. Sci. U.S.A. 100, 13881–13886.
[4] Wiseman, B., Carpena, X., Feliz, M., Donald, L.J., Pons, M., Fita, I. and Loewen, P.C. (2010) Isonicotinic acid hydrazide conversion to isonicotinyl-NAD by catalase–peroxidases. J. Biol. Chem. 285, 26662–26673.
[5] Yu, S., Girotto, S., Lee, C. and Magliozzo, R.S. (2003) Reduced affinity for isoniazid in the S315T mutant of *Mycobacterium tuberculosis* KatG is a key factor in antibiotic resistance. J. Biol. Chem. 278, 14769–14775.
[6] Zhao, X., Yu, H., Yu, S., Wang, F., Sacchettini, J.C. and Magliozzo, R.S. (2006) Hydrogen peroxide-mediated isoniazid activation catalyzed by *Mycobacterium tuberculosis* catalase–peroxidase (KatG) and its S315T mutant. Biochemistry 45, 4131–4140.
[7] Suarez, J., Ranguelova, K., Schelvis, J.P. and Magliozzo, R.S. (2009) Antibiotic resistance in *Mycobacterium tuberculosis*: peroxidase intermediate bypass causes poor isoniazid activation by the S315G mutant of *M. tuberculosis* catalase–peroxidase (KatG). J. Biol. Chem. 284, 16146–16155.
[8] Donald, L.J., Krokhin, O.V., Duckworth, H.W., Wiseman, B., Deemagarn, T., Singh, R., Switala, J., Carpena, X., Fita, I. and Loewen, P.C. (2003) Characterization of the catalase–peroxidase KatG from *Burkholderia pseudomallei* by mass spectrometry. J. Biol. Chem. 278, 35687–35692.
[9] Deemagarn, T., Carpena, X., Singh, R., Wiseman, B., Fita, I. and Loewen, P.C. (2005) Structural characterization of the Ser324Thr variant of the catalase–peroxidase (KatG) from *Burkholderia pseudomallei*. J. Mol. Biol. 345, 21–28.
[10] Vidossich, P., Loewen, P.C., Carpena, X., Fiorin, G., Fita, I. and Rovira, C. (2014) Binding of the antitubercular pro-drug isoniazid in the heme access channel of catalase–peroxidase (KatG). A combined structural and metadynamics investigation. J. Phys. Chem. B 118, 2924–2931.
[11] Ivancich, A., Jakopitsch, C., Auer, M., Un, S. and Obinger, C. (2003) Protein-based radicals in the catalase–peroxidase of *Synechocystis* PCC6803: a multifrequency EPR investigation of wild-type and variants on the environment of the heme active site. J. Am. Chem. Soc. 125, 14093–14102.
[12] Jakopitsch, C., Obinger, C., Un, S. and Ivancich, A. (2006) Identification of Trp106 as the tryptophanyl radical intermediate in *Synechocystis* PCC6803 catalase–peroxidase by multifrequency Electron Paramagnetic Resonance spectroscopy. J. Inorg. Biochem. 100, 1091–1099.
[13] Colin, J., Jakopitsch, C., Obinger, C. and Ivancich, A. (2010) The reaction of synechocystis catalase–peroxidase (KatG) with isoniazid investigated by multifrequency (9–285 GHz) EPR spectroscopy. Appl. Magn. Reson. 37, 267–277.
[14] Kamachi, S., Hirayabashi, K., Tamoi, M., Shigeoka, S., Tada, T. and Wada, K. (in press) The crystal structure of isoniazid-bound KatG catalase–peroxidase from *Synechococcus elongatus* PCC7942. FEBS J.
[15] Carpena, X., Loprasert, S., Mongkolsuk, S., Switala, J., Loewen, P.C. and Fita, I. (2003) Catalase–peroxidase KatG of *Burkholderia pseudomallei* at 1.7 Å resolution. J. Mol. Biol. 327, 475–489.
[16] Bertrand, T., Eady, N.A., Jones, J.N., Jesmin, Nagy, J.M., Jamart-Gregoire, B., Raven, E.L. and Brown, K.A. (2004) Crystal structure of *Mycobacterium tuberculosis* catalase-peroxidase. J. Biol. Chem. 279, 38991–38999.
[17] Kamachi, S., Wada, K., Tamoi, M., Shigeoka, S. and Tada, T. (2014) The 2.2 Å resolution structure of the catalase–peroxidase KatG from *Synechococcus elongatus* PCC7942. Acta Crystallogr. F Struct. Biol. Commun. 70, 288–293.
[18] Lukat-Rodgers, G.S., Wengenack, N.L., Rusnak, F. and Rodgers, K.R. (2001) Carbon monoxide adducts of KatG and KatG(S315T) as probes of the heme site and isoniazid binding. Biochemistry 40, 7149–7157.
[19] Wengenack, N.L., Todorovic, S., Yu, L. and Rusnak, F. (1998) Evidence for differential binding of isoniazid by *Mycobacterium tuberculosis* KatG and the isoniazid-resistant mutant KatG(S315T). Biochemistry 37, 15825–15834.
[20] Singh, R., Switala, J., Loewen, P.C. and Ivancich, A. (2007) Two [Fe(IV)═O Trp$^{+}$] intermediates in *M. tuberculosis* catalase–peroxidase discriminated by multifrequency (9–285 GHz) EPR spectroscopy: reactivity toward isoniazid. J. Am. Chem. Soc. 129, 15954–15963.
[21] Yamada, Y., Fujiwara, T., Sato, T., Igarashi, N. and Tanaka, N. (2002) The 2.0 Å crystal structure of catalase–peroxidase from *Haloarcula marismortui*. Nat. Struct. Biol. 9, 691–695.
[22] Wada, K., Tada, T., Nakamura, Y., Kinoshita, T., Tamoi, M., Shigeoka, S. and Nishimura, K. (2002) Crystallization and preliminary X-ray diffraction studies of catalase–peroxidase from *Synechococcus* PCC 7942. Acta Crystallogr. D Biol. Crystallogr. 58, 157–159.
[23] Otwinowsky, Z. and Minor, W. (1997) Processing of X-ray diffraction data collected in oscillation mode. Methods Enzymol. 276, 307–326.
[24] Murshudov, G.N., Vagin, A.A. and Dodson, E.J. (1997) Refinement of macromolecular structures by the maximum-likelihood method. Acta Cryst. D53, 240–255.
[25] N. Collaborative Computational Project (1994) The CCP4 suite: programs for protein crystallography. Acta Cryst. D50, 760–763.
[26] Emsley, P. and Cowtan, K. (2004) Coot: model-building tools for molecular graphics. Acta Cryst. D60, 2126–2132.
[27] Pierattelli, R., Banci, L., Eady, N.A., Bodiguel, J., Jones, J.N., Moody, P.C., Raven, E.L., Jamart-Gregoire, B. and Brown, K.A. (2004) Enzyme-catalyzed mechanism of isoniazid activation in class I and class III peroxidases. J. Biol. Chem. 279, 39000–39009.
[28] Metcalfe, C., Macdonald, I.K., Murphy, E.J., Brown, K.A., Raven, E.L. and Moody, P.C. (2008) The tuberculosis prodrug isoniazid bound to activating peroxidases. J. Biol. Chem. 283, 6193–6200.
[29] Gumiero, A., Murphy, E.J., Metcalfe, C.L., Moody, P.C. and Raven, E.L. (2010) An analysis of substrate binding interactions in the heme peroxidase enzymes: a structural perspective. Arch. Biochem. Biophys. 500, 13–20.
[30] Patterson, W.R., Poulos, T.L. and Goodin, D.B. (1995) Identification of a porphyrin π cation radical in ascorbate peroxidase compound I. Biochemistry 34, 4342–4345.
[31] Colin, J., Wiseman, B., Switala, J., Loewen, P.C. and Ivancich, A. (2009) Distinct role of specific tryptophans in facilitating electron transfer or as [Fe(IV)═O Trp($^{+}$)] intermediates in the peroxidase reaction of *Burkholderia pseudomallei* catalase–peroxidase: a multifrequency EPR spectroscopy investigation. J. Am. Chem. Soc. 131, 8557–8563.
[32] Sharp, K.H., Mewies, M., Moody, P.C. and Raven, E.L. (2003) Crystal structure of the ascorbate peroxidase-ascorbate complex. Nat. Struct. Biol. 10, 303–307.
[33] Itakura, H., Oda, Y. and Fukuyama, K. (1997) Binding mode of benzhydroxamic acid to *Arthromyces ramosus* peroxidase shown by X-ray crystallographic analysis of the complex at 1.6 Å resolution. FEBS Lett. 412, 107–110.
[34] Henriksen, A., Schuller, D.J., Meno, K., Welinder, K.G., Smith, A.T. and Gajhede, M. (1998) Structural interactions between horseradish peroxidase C and the substrate benzhydroxamic acid determined by X-ray crystallography. Biochemistry 37, 8054–8060.
[35] Tsukamoto, K., Itakura, H., Sato, K., Fukuyama, K., Miura, S., Takahashi, S., Ikezawa, H. and Hosoya, T. (1999) Binding of salicylhydroxamic acid and several aromatic donor molecules to *Arthromyces ramosus* peroxidase, investigated by X-ray crystallography, optical difference spectroscopy, NMR relaxation, molecular dynamics, and kinetics. Biochemistry 38, 12558–12568.
[36] Sharp, K.H., Moody, P.C., Brown, K.A. and Raven, E.L. (2004) Crystal structure of the ascorbate peroxidase–salicylhydroxamic acid complex. Biochemistry 43, 8644–8651.